Radboud Repository

Radboud University Nijmegen

PDF hosted at the Radboud Repository of the Radboud University Nijmegen

This full text is a publisher's version.

For additional information about this publication click this link.
http://hdl.handle.net/2066/29753

Please be advised that this information was generated on 2014-11-19 and may be subject to change.

Two-dimensional distributions of C_2, CH, and OH in a diamond depositing oxyacetylene flame measured by laser induced fluorescence

R. J. H. Klein-Douwel,[a] J. J. L. Spaanjaars, and J. J. ter Meulen
Department of Molecular and Laser Physics, University of Nijmegen, Toernooiveld, 6525 ED Nijmegen, The Netherlands

(Received 27 January 1995; accepted for publication 20 April 1995)

Two-dimensional laser induced fluorescence measurements are applied to the chemical vapor deposition of diamond by an oxyacetylene flame. The fluorescence distributions of C_2, CH, and OH are measured for various deposition conditions. The influence of the temperature of the molybdenum substrate and the distance between the substrate and the flame front on the two-dimensional distributions and on the quality and morphology of the deposited diamond is investigated. A relation is observed between the C_2 distribution in the flame and the local growth rate and quality of the diamond layer, therefore C_2 is thought to be an important species for diamond growth. The exact role of CH as a growth species is less clear; OH seems to be of minor importance. All measurements are performed during diamond deposition. © *1995 American Institute of Physics.*

I. INTRODUCTION

Diamond deposition by a flame probably dates back to the development of the first burners, their inventors not knowing they might have deposited diamond among the soot they produced. In 1988 Hirose and Kondo[1] reported diamond deposition obtained with a laminar oxyacetylene flame, operated with a small excess of acetylene. The technique of diamond deposition by a laminar flame is well established by now and deposition rates exceeding 100 μm/h[2,3] with a quality comparable to that of natural type IIa diamond[3,4] are reported.

Up till now many experiments have been performed on the gas phase of the flame in order to study the processes leading to diamond deposition. The experiments include optical emission spectroscopy (OES) of C_2, CH, and OH[5–7] and various laser based techniques, among which laser induced fluorescence (LIF) detection of C_2 and OH[8] and planar laser induced photodissociation fluorescence of CH.[9] These and other optical diagnostic tools have also been used for characterization of other diamond chemical vapor deposition (CVD) processes, e.g., OES of H, H_2, C, C_2, CH, O, and OH[10] and degenerate four wave mixing (DFWM) detection of C_2 and CH[11] in a microwave plasma; LIF detection has been applied to C_2 and CH in a dc arcjet plasma[12] and to H in a hot filament CVD reactor.[13,14]

OES measurements provide evidence about the presence of various species in excited electronic states in the reaction system. Hirose *et al.*[6] have found the relative OH emission intensity in the flame to be higher under "high-quality diamond" growth conditions than under "ordinary opaque diamond" growth conditions. Okada and co-workers[7] determined vertical profiles for the emission intensity of C_2, CH, and OH. They found the C_2 and CH emission to decrease with increasing distance from the burner tip, but the OH emission to remain constant.

A limitation of OES, however, is that it only probes excited state species, whereas ground state species are also important for diamond growth. An often applied method to probe species state selectively is the LIF detection technique. Using this technique the detected species is unambiguously identified by its excitation spectrum and undesired signals often can be filtered out. Furthermore, the LIF signal is directly proportional to the density in the probed lower state of the specific molecule under investigation. A problem often encountered in quantifying LIF signals is the quenching of fluorescence by collisions with other molecules present in the system. Certainly in flames used at atmospheric pressure collisional quenching cannot be neglected.

The problem of the OES method being a line of sight integrating technique is avoided by the LIF technique, where the laser beam is focused in a small volume. Matsui *et al.*[8] have obtained lateral profiles of C_2 and OH in an oxyacetylene flame, determined by LIF, for various distances from the burner tip.

Many experiments on gas phase diagnostics of diamond CVD processes have been restricted to point[6,7,11–14] or line[8] measurements, which makes it difficult to determine two-dimensional distributions of the species of interest. Also many measurements have been carried out without the actual substrate in place,[5–8,12] in which case the gas phase composition, temperature, and dynamics are strongly different from diamond deposition conditions. For the oxyacetylene flame, for instance, the substrate temperature is about 1700 K or more lower than the temperature at the flame front, and therefore a large temperature gradient exists in the region just above the substrate. Detailed calculations by Matsui *et al.*[15] and Goodwin[16] show that the concentration of many important species changes very rapidly close to the substrate. Cappelli and Paul[9] have performed two-dimensional measurements, but did not detect species closer than 1 mm to the substrate.

The two-dimensional LIF technique is widely used as a combustion diagnostics tool, because it allows high resolution, non-intrusive, sensitive, state selective, *in situ* measure-

[a]Electronic mail: robertkd@sci.kun.nl

 0021-8979/95/78(3)/2086/11/$6.00 © 1995 American Institute of Physics

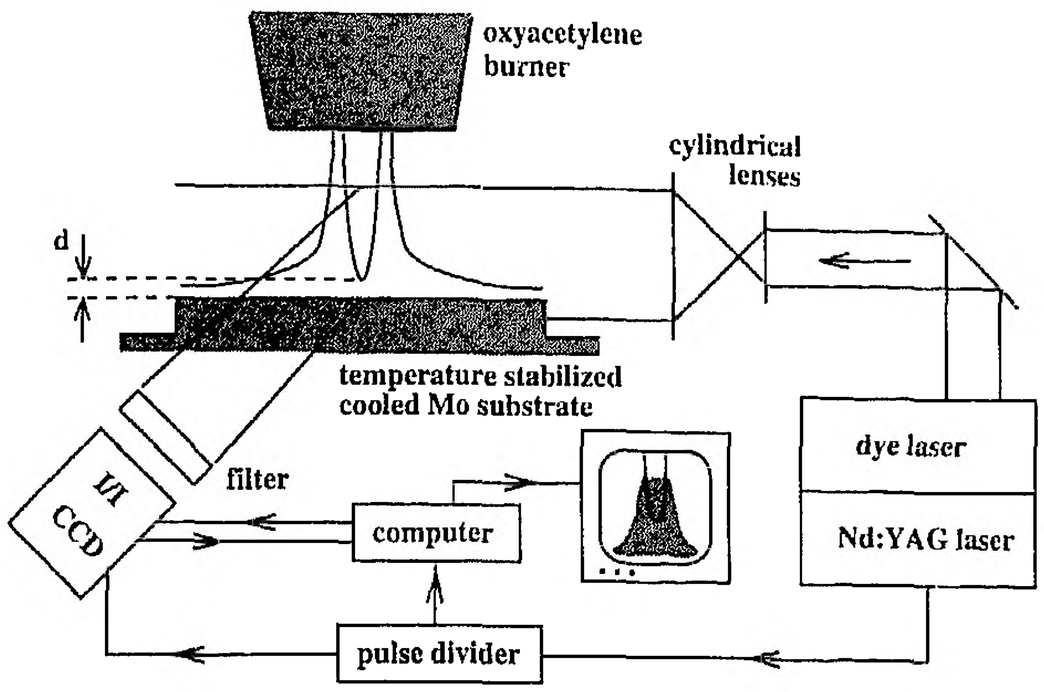

FIG. 1. Schematic overview of the experimental setup, showing welding torch, cooled substrate, laser, CCD camera with image intensifier (I/I), and computer. The temperature stabilization is not shown.

ments of a large variety of species in a wide range of environments: flames ranging from millimeters (this work) to meters[17] in size, and from low pressure flames[18] to the adverse combustion environment inside a running Diesel engine.[19] In this work the 2D-LIF method is applied to the diamond depositing oxyacetylene flame in order to gain insight in the gas phase chemistry and the deposition process. Knowledge about the chemistry and dynamics of the dominant diamond precursors is indispensable for the optimization and upscaling of the flame deposition setup. LIF signals of these precursors may also be used to automate the deposition process and allow large scale, stable diamond growth.

The LIF distributions of C_2, CH, and OH during diamond deposition are measured in this work. The relation between the quality and morphology of the deposited diamond layers and the distributions of these species in the boundary layer is studied for various deposition conditions.

II. EXPERIMENT

A. Diamond deposition

The flame deposition setup used to deposit diamond layers has been described by Schermer *et al.*[20] but major details are given here for ease of reference. A commercially available welding torch, equipped with a burner tip with an orifice of 1.6 mm ϕ, is used to produce a laminar flame by burning high purity acetylene (99.6%) with oxygen (99.995%). A molybdenum substrate is positioned perpendicularly to the flame axis at a distance d below the tip of the flame front, as shown in Fig. 1. The distance d, which is typically 1 mm, can be adjusted with an accuracy of 0.1 mm and is determined with a cathetometer and a CCD camera. The substrate is soldered onto a molybdenum substrate holder, which is clamped onto a stainless steel cooler equipped with a pulsed water spray unit. A thermocouple measures the temperature T_s at approximately 2.5 mm below the center of the substrate surface. A temperature controller, connected with the thermocouple, is used to regulate the water valve. In this way T_s is kept constant to ± 1°C. The actual growth temperature T_d at the substrate surface is not exactly known, but from previous studies using an IR two-color pyrometer[20,21] it is known that $T_d \approx T_s + 150$ °C for all deposition experiments described in this work.

During the experiment the gas flows are kept constant by means of mass flow controllers. The oxygen flow is 2.84 ± 0.02 standard liters per minute (SLM). The acetylene flow is determined by the acetylene supersaturation S_{ac}, needed for diamond deposition. S_{ac} is defined as the percentage of extra acetylene flow compared to the acetylene flow of a neutral flame. The neutral flame is neither oxygen-rich nor fuel-rich and shows a distinct, conical flame front. An overmeasure of acetylene causes a so-called acetylene feather to form outside the flame front. The disappearance of the bright feather occurs at an acetylene flow for which $S_{ac} = 0\%$ and is determined by sight and also more accurately by LIF detection (as discussed below). S_{ac} is used as parameter for the acetylene flow, rather than the absolute acetylene-to-oxygen flow ratio R,[8] because in contrast to S_{ac} the flow ratio R is known to depend on the total flow, the burner orifice diameter, the geometry of the burner and the temperature of the burner head. In all experiments $S_{ac}=5\%$ is used, unless stated otherwise. T_s is varied from one deposition experiment to another between 850 and 1150 °C and d is varied between 0.58 and 1.99 mm.

The molybdenum substrates used are 12 mm×12 mm square and 0.5 mm thick. They are scratched with micrometer sized diamond powder, prior to deposition, to enhance diamond nucleation. The deposition time in all experiments is about one hour. The influence of the key parameters T_s, d, and S_{ac} on the growth rate, quality and morphology of the deposited diamond has been described in detail by Schermer and co-workers.[20]

B. Two-dimensional LIF

A system consisting of a pulsed tunable laser and a CCD camera with image intensifier is used to perform *in situ* two-dimensional LIF measurements in the flame. The species under investigation are probed with a dye laser, pumped with the second or third harmonic of a Nd:YAG laser, operating at 10 Hz. The time duration of the laser pulse is 5 ns and the power is kept low enough to avoid saturation of the specific molecular transition induced. Pulse to pulse fluctuations in the laser power are eliminated by averaging over 10 laser shots. The laser beam is transformed into a laser sheet by two cylindrical lenses, resulting in a cross section 4 mm high ×0.1 mm wide in the flame. Due care is taken to obtain a homogeneous laser beam profile in the vertical direction.

The laser sheet is directed through the center of the flame and the fluorescence is collected at right angles by the CCD camera. The inhomogeneous lower edge of the laser beam is directed to just below the substrate and is therefore cut off. In order to obtain the highest possible spatial resolution, expandable bellows are mounted between the camera and the camera objective. For LIF detection of C_2 and CH, a Micro-Nikkor 200 mm f/4.0 objective is used with the maximum expansion of 16 cm of the bellows, giving a spatial resolution of 20 μm per image line. For LIF detection of OH, which takes place in the ultraviolet, a UV-Nikkor 105

mm f/4.5 objective is used, with bellows 5 cm expanded, resulting in a spatial resolution of 40 μm.

Images are acquired with a Peltier cooled CCD camera equipped with an image intensifier, all comprised in one unit, and digitized with the accompanying A/D converter installed in a personal computer. Image processing is done with the corresponding software package and is used for background subtraction and recording of spectra. Image acquisition is triggered by feeding the trigger of the Q-switch of the Nd:YAG laser into a pulse divider/transformer, which triggers the image intensifier and the computer. The computer triggers the actual integration of the CCD chip and simultaneously acts as a pulse counter, thus allowing on-chip integration of multiple laser shots. This is used to improve the signal to noise ratio if signals are weak. The image intensifier is gated 15 ns and is switched on when the laser pulse intersects the flame. In this way the natural emission of the flame is suppressed by a factor 7×10^6.

Background subtraction is applied to all measurements to eliminate the remaining natural emission of the flame and possible non-resonant fluorescence. First, an image is obtained with the laser tuned exactly to the transition of interest and immediately afterwards an image is obtained with the laser tuned off resonance. The only difference between these two images is the fluorescence of the molecule under investigation, which is therefore obtained by subtracting the resonant and off resonant images.

In order to avoid saturation of the image intensifier caused by reflections of the laser beam from the substrate and substrate holder, fluorescence has to be detected off-resonant and cut-off filters have to be used. C_2 is detected by exciting the $d^3\Pi_g(v'=2)\leftarrow a^3\Pi_u(v''=0)$ transition around 438 nm (Swan system). A long-pass filter transmitting only $\lambda \geqslant 470$ nm is used, which allows the detection of the $d^3\Pi_g(v')\rightarrow a^3\Pi_u(v'')$ fluorescence for v' up to 4.[22] Fluorescence from the $v' \neq 2$ levels is due to collisional redistribution of population in the $d^3\Pi_g$ state.

CH is excited at the $B^2\Sigma^-(v'=0)\leftarrow X^2\Pi(v''=0)$ transition at 393 nm. Because the $B^2\Sigma^-$ and the $A^2\Delta$ states cross each other, strong collisional redistribution between these two states takes place and fluorescence from the $A^2\Delta$ $(v'=0) \rightarrow X^2\Pi(v''=0)$ transition can be observed around 431 nm.[23] A Schott KV 418 filter is used to block reflections of the laser beam and is combined with a narrow bandpass filter (maximum transmission at 431 nm and 16 nm FWHM) to block non-resonant background fluorescence.

Because the Franck-Condon factors for $\Delta v \neq 0$ transitions are typically <0.01,[24] excitation of the $A^2\Delta(v'=0)\leftarrow X^2\Pi(v''=0)$ transition results in resonant fluorescence around 431 nm. Initial attempts to excite CH at 431 nm yielded fluorescence which could be identified as the C_2 Swan system described above. This C_2 fluorescence around 431 nm is strong enough to prevent any CH fluorescence feature from being detected. Resonant detection of CH is also hampered by strong emission at 431 nm of the flame itself, caused by naturally abundant excited CH. Excitation of the $C^2\Sigma^+(v'=0)\leftarrow X^2\Pi(v''=0)$ transition of CH around 315 nm is not used, because of strong predissociation in the excited state.[25]

LIF detection of OH is carried out by excitation of the $A^2\Sigma^+(v'=1)\leftarrow X^2\Pi(v''=0)$ transition at 282 nm. Resonant fluorescence and laser reflections are cut off by a Schott WG 305 filter, which transmits the $1\rightarrow1$ fluorescence at 312 nm. Excitation of OH is also possible at 308 nm ($0\leftarrow 0$), but this only leaves the much weaker $0\rightarrow1$ fluorescence at 343 nm for off resonant detection, using a Schott WG 335 filter. Another interesting detection scheme for OH is excitation at 248 nm ($3\leftarrow0$) and detection at 295 nm ($3\rightarrow2$). Due to predissociation in the $A^2\Sigma^+(v'=3)$ state, fluorescence will not be influenced by collisional quenching. This detection scheme can therefore be used to determine the temperature in the flame.[26] The signals being very weak, however, compared to the other two detection schemes for OH mentioned above, this transition is not used for measurements presented in this work.

Quantitative analysis of the LIF signals is hampered by quenching of the fluorescence due to inelastic collisions of the excited molecules. This quenching depends strongly on the pressure, temperature and collision partners, and is therefore expected to be different in different regions of the flame. The quantitative dependence is not known, so that the LIF results can only be interpreted in a more qualitative way.

C. Characterization of the deposited diamond

Because molybdenum substrates are used in all experiments, the deposited diamond is of polycrystalline nature. After growth the diamond layers are characterized by optical microscopy, Raman spectroscopy, and Scanning Electron Microscopy (SEM).

The thickness of the diamond layer is determined by focusing the optical microscope with an accuracy of ±2 μm at different positions at the deposited diamond layer and at the edge of the substrate, where no deposition has taken place. The exact procedure is described in detail by Schermer *et al.*[20] The thickness measurements combined with the total deposition time give the growth rate v_d.

Raman spectra are taken at radially different positions for each diamond layer by focusing an Ar^+ laser beam to a spot size of ≈30 μm. In order to quantify the quality of the layer a quality factor Q is used: it is defined as 1000 times the area of the diamond peak in the Raman spectrum divided by the area of the background between 1100 and 1700 cm^{-1}.[20] High Q values correspond to high purity diamond, whereas low Q values indicate a high non-diamond carbon content and/or a high fluorescence background of the deposited layer.

III. RESULTS

A. Two-dimensional mapping of species in the flame

The two-dimensional fluorescence distributions of the species of interest are measured in the flame while diamond is growing on the substrate surface. The deposition parameters are kept constant during each growth experiment. Weak reflections of the flame and of the laser induced fluorescence in the substrate holder can be seen in every image, but because these are below the substrate, the reflections do not influence the measurements.

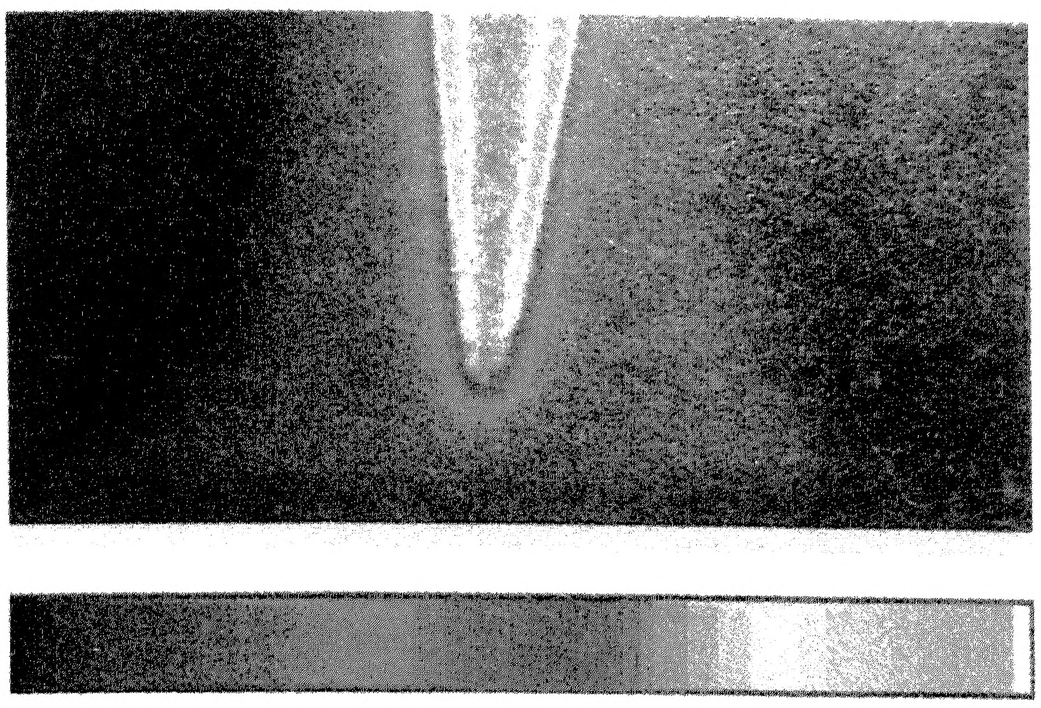

FIG. 2. Natural emission ≥470 nm (mainly C_2) of the flame during diamond deposition (T_s=1000 °C, d=0.88 mm). False colors are used to indicate intensities; the image is 8 mm wide. The substrate is indicated in yellow; the burner tip is located just outside the image.

In the volume of interest a pressure gradient and a large temperature gradient exist between the flame and the substrate. This might give rise to diffraction of light by the corresponding gradient in index of refraction, the so-called mirage effect. A small effect is observed when the unfocused beam of a HeNe laser is directed through the conical flame front. It is checked carefully, however, that the beam of the dye laser, which is focused into a laser sheet, shows no observable deviation caused by the flame. Therefore the mirage effect can be neglected in interpreting the images recorded in the flame.

Figure 2 shows the natural emission of the flame (laser off) during diamond deposition for λ≥470 nm, which mainly consists of C_2 emission lines.[5] The conical flame front can be clearly seen, together with the acetylene feather, which spreads outward as the flame impinges on the substrate. The exact vertical position of the tip of the flame front is determined by taking an intensity profile of the natural flame emission along the symmetry axis of the flame, as shown in Fig. 3(a). The tip of the flame front is here defined to be at the half maximum point in the intensity profile. The substrate

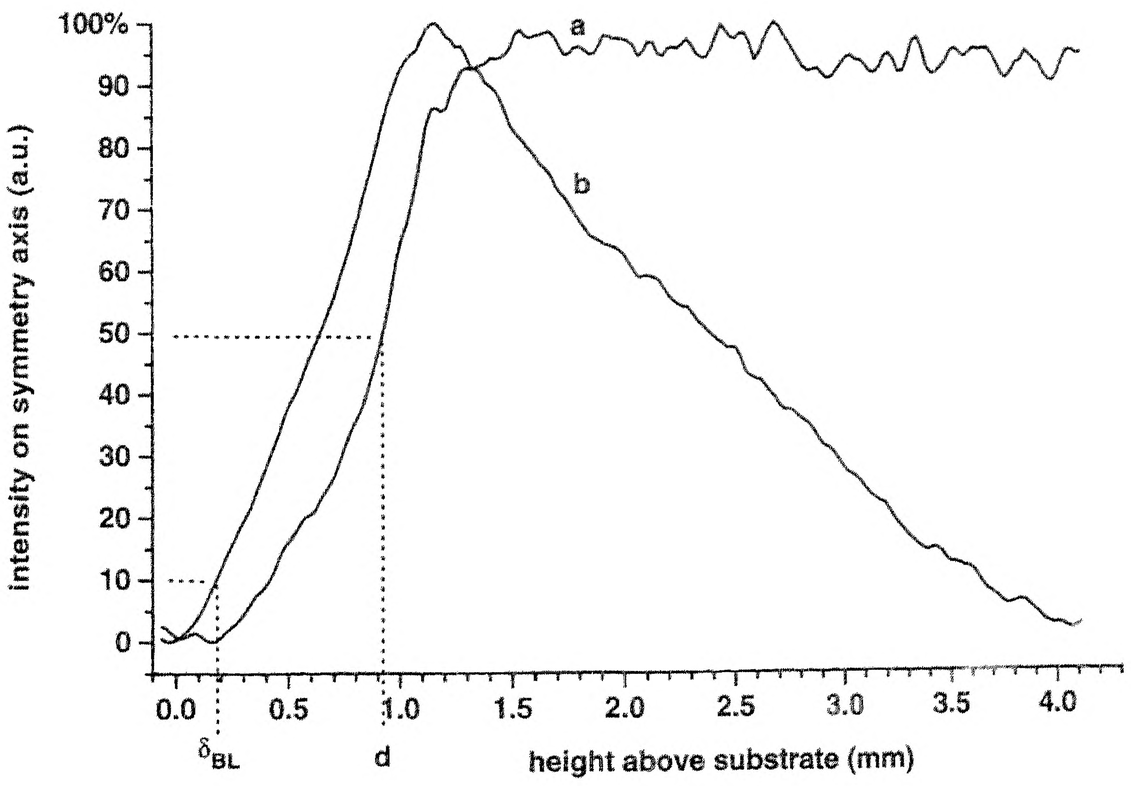

FIG. 3. Intensity profiles along the symmetry axis of the flame: (a) natural flame emission (obtained from Fig. 2); (b) C_2 LIF signal [obtained from Fig. 5(a)]. The method for determining d and δ_{BL} is indicated.

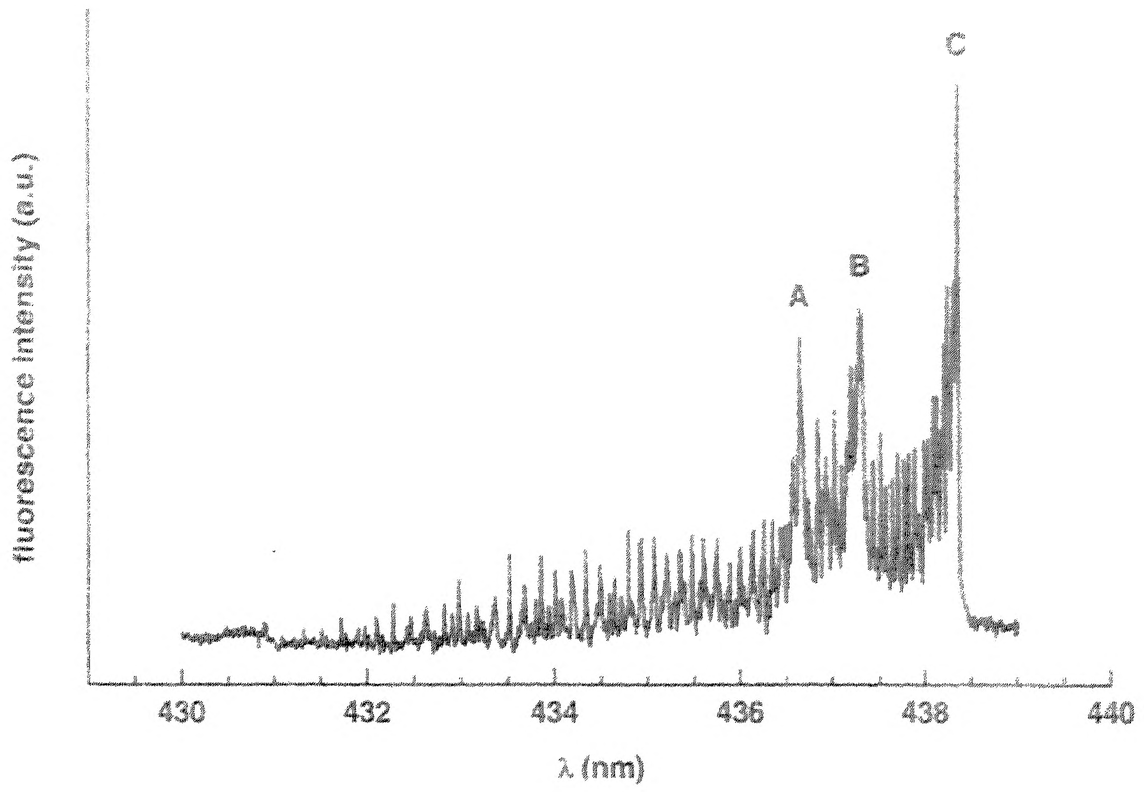

FIG. 4. Excitation spectrum of the C_2 Swan band, recorded just below the flame front during diamond deposition. The band head marked with 'C' is used for imaging.

surface is located at the point of minimum intensity. In this way the distance d is determined with an accuracy of 70 μm.

1. C_2

The C_2 excitation spectrum, presented in Fig. 4, is recorded in the acetylene feather, just below the flame front. The small background in the spectrum is due to the not completely suppressed natural emission of the flame. Figure 5 shows the C_2 LIF distribution at various distances d. Upon inspection of these figures it is clear that the highest LIF intensity of C_2 is found at the flame front, and also that the

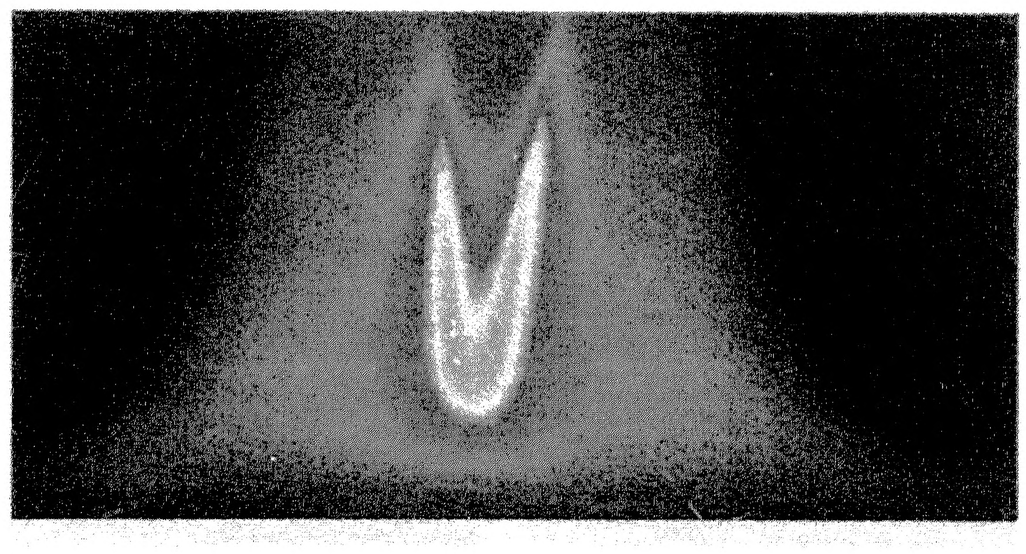

(a)

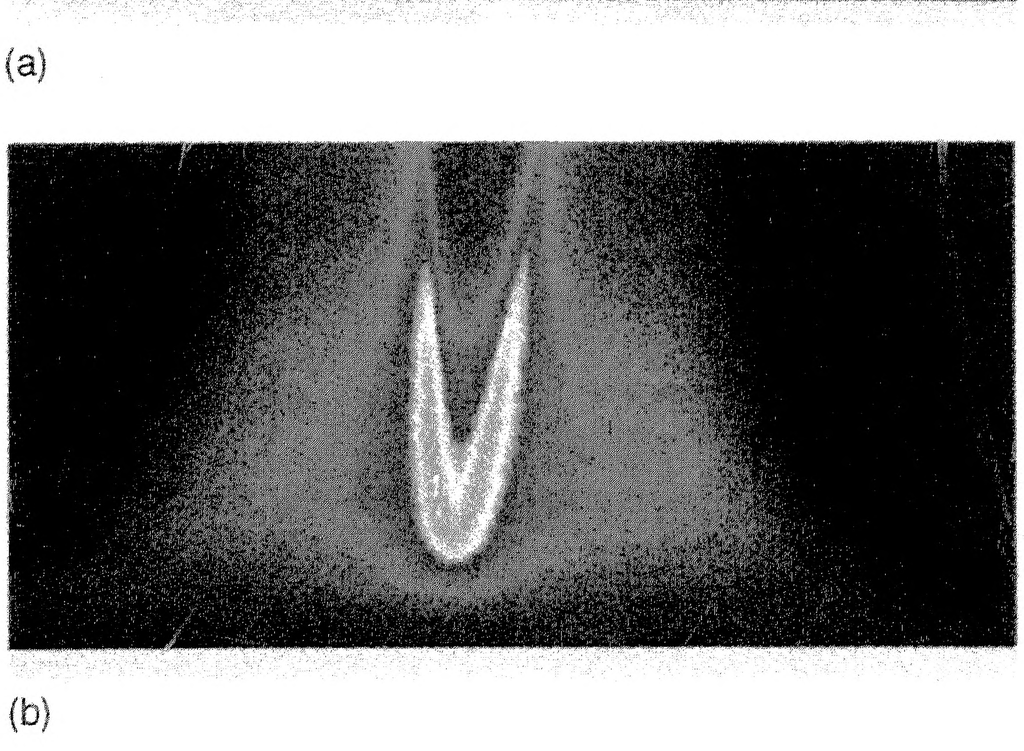

(b)

FIG. 5. C_2 LIF distributions during diamond deposition for various growth conditions. The substrate is indicated in yellow; the images are 8 mm wide. S_{ac}=5%, T_s=1000 °C, and d=0.88 mm (a) and 0.58 mm (b), respectively.

entire acetylene feather is filled with C_2, as can be expected from the combustion reaction mechanisms.[27] The C_2 signal decreases strongly in going from the flame front to the substrate, as is shown in Fig. 3(b). A dark boundary layer can be distinguished in all distributions, of both LIF and natural emission.

In order to study the boundary layer as a function of deposition parameters, the thickness δ_{BL} of the boundary layer is defined here as the distance between the substrate surface and the position where the emission intensity (LIF or natural emission) is 10% of the maximum intensity. Each value of δ_{BL} is determined separately from the corresponding intensity profile along the symmetry axis of the flame, as shown in Fig. 3(b). The dependence of δ_{BL} on T_s and d for both the LIF and the natural emission is shown in Fig. 6: δ_{BL} remains nearly constant with changing T_s, but increases slightly with increasing d.

Figure 5 reveals that the boundary layer is not strictly flat, but shows different structures for different deposition conditions. Horizontal C_2 LIF intensity profiles are measured for diamond deposition at various distances d, as shown in Fig. 7, while T_s and S_{ac} are kept constant at 1000 °C and 5%, respectively. Each horizontal profile is taken at a distance δ_{BL} above the substrate. From Fig. 7 it is clear that the profiles show a single maximum at the symmetry axis of the flame for d<1 mm, but that a shallow minimum appears in the C_2 LIF intensity for d>1 mm.

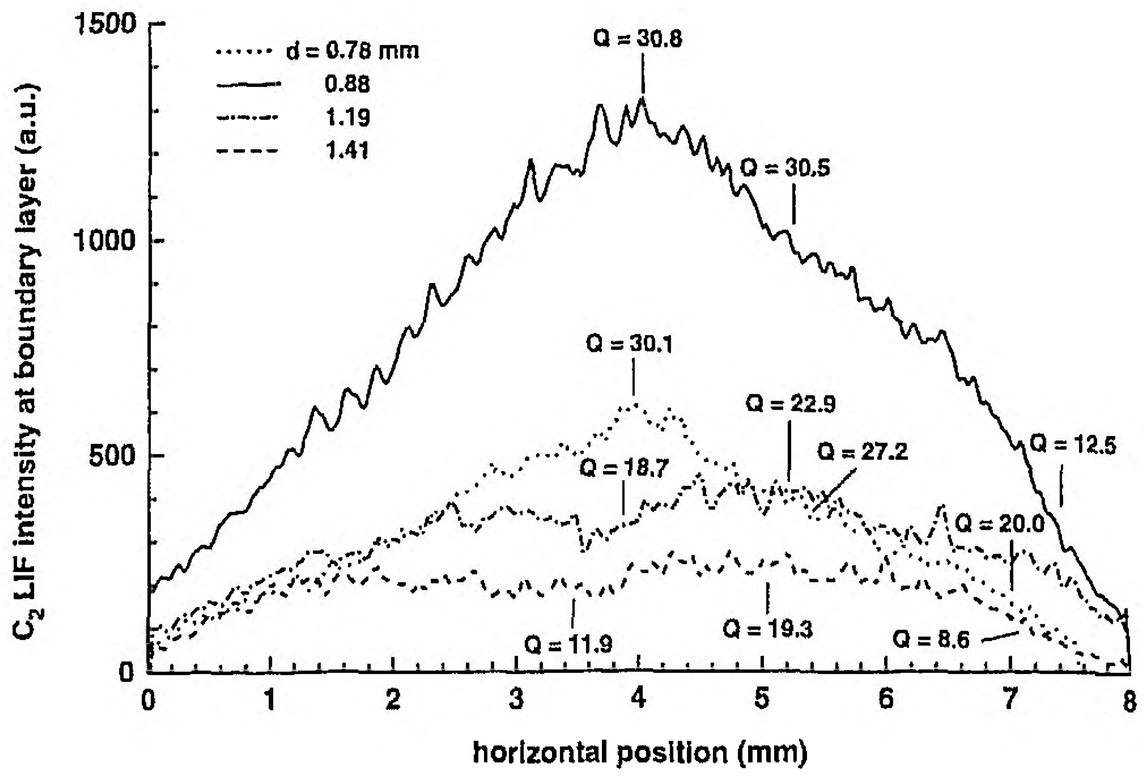

FIG. 7. Horizontal C_2 LIF intensity profiles at a distance δ_{BL} above the substrate, for different deposition distances; T_s =1000 °C. Q is the quality factor of the diamond deposit at the corresponding position at the substrate.

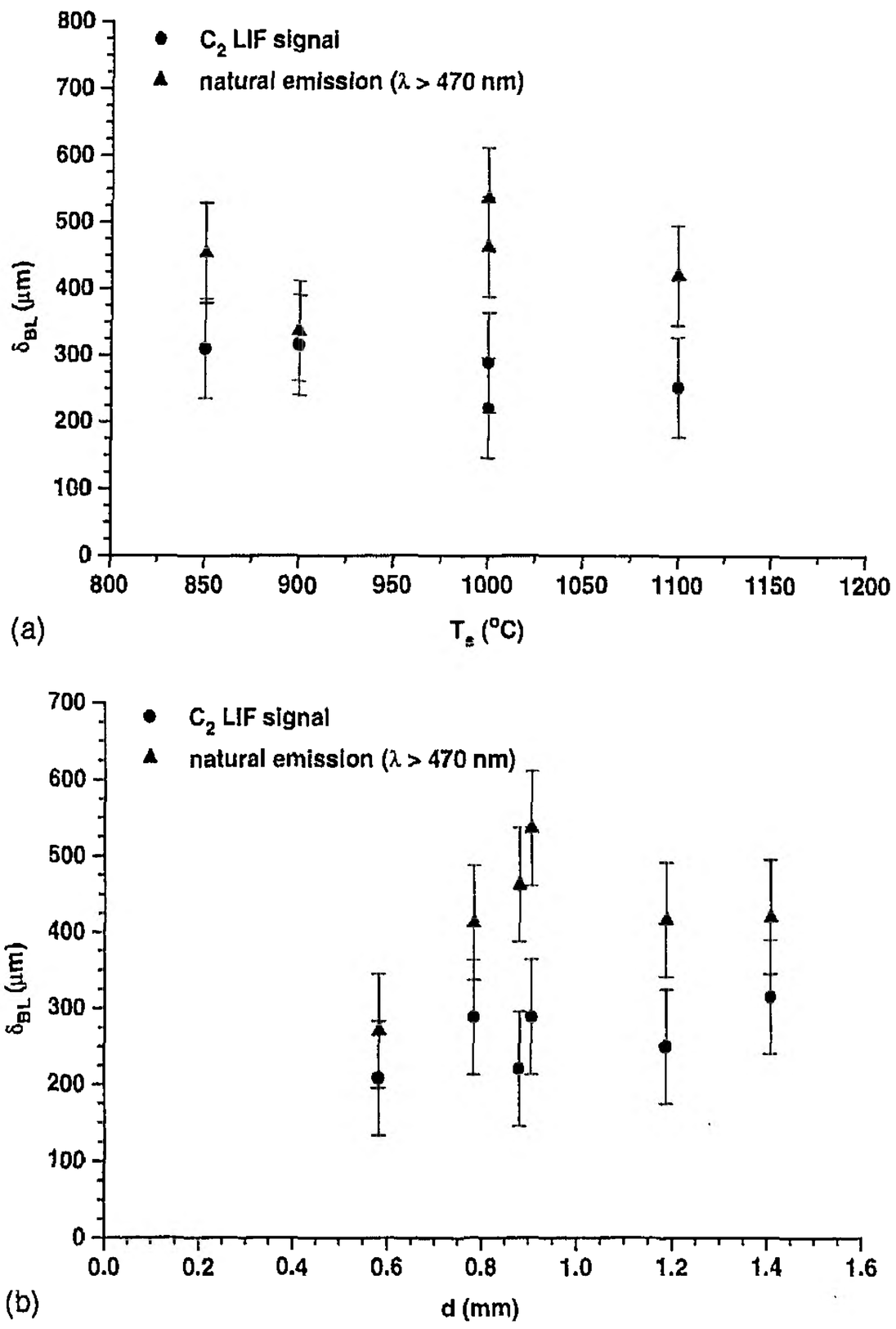

FIG. 6. Dependence of the thickness of the boundary layer δ_{BL} on (a) the temperature T_s and (b) the distance d for C_2 LIF and natural emission.

Comparison of Figs. 2 and 5a, which are recorded immediately after one another during the same deposition experiment, shows that the natural emission of the flame is in all directions confined to a smaller area than the LIF distribution of C_2. This is reflected in the larger values for δ_{BL} in natural emission as compared to δ_{BL} for the C_2 LIF distribution, shown in Fig. 6, with all deposition conditions the same. This is probably related to the fact that the natural emission of the flame for $\lambda \geqslant 470$ nm is mostly caused by chemiluminescence from the excited $d^3\Pi_g$ state of C_2, whereas the LIF technique probes the lower lying $a^3\Pi_u$ state.

2. CH

For CH similar experiments have been carried out as for C_2. Figure 8 shows the natural CH emission of the flame at 431 nm, while diamond is being deposited, and Fig. 9 shows the excitation spectrum of CH, recorded at the tip of the flame front. The large background in the excitation spectrum is due to non-resonant fluorescence, probably from polyacetylenes and other large hydrocarbons which are formed in the combustion in the fuel-rich flame.[28] This non-resonant signal turns out to be directly proportional to the laser power. The background in the excitation spectrum therefore reflects the gain profile of the dye laser. The constant offset is caused by the natural CH emission of the flame.

In Fig. 10 the two-dimensional distribution of the CH LIF signal during diamond deposition is shown. Because the absolute intensity of the CH LIF signal is lower than that of the C_2 LIF signal and the optical quality of the CH narrow bandpass filter is less than that of the long-pass filter used for C_2, the signal to noise ratio for the CH LIF images is less than for the C_2 LIF images. Some strong reflections of the laser beam, caused by facets of the growing diamond crystallites, are visible because they are not completely blocked by the filter combination used. The CH LIF distribution

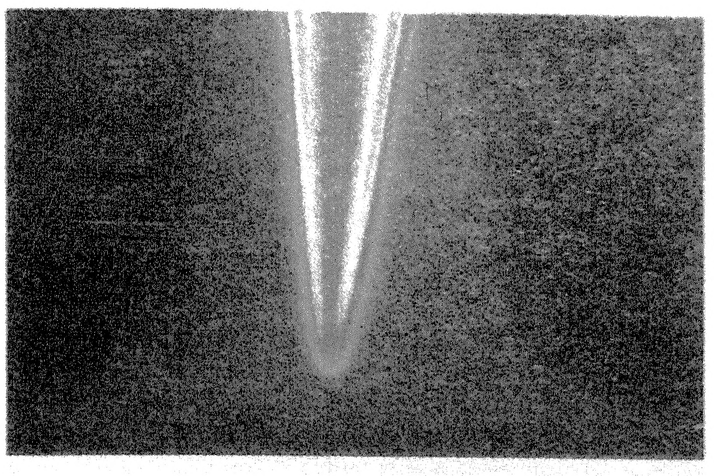

FIG. 8. Natural CH emission of the flame around 431 nm during diamond deposition (T_s=1000 °C, d=0.95 mm). The substrate is indicated in yellow; the image is 8 mm wide.

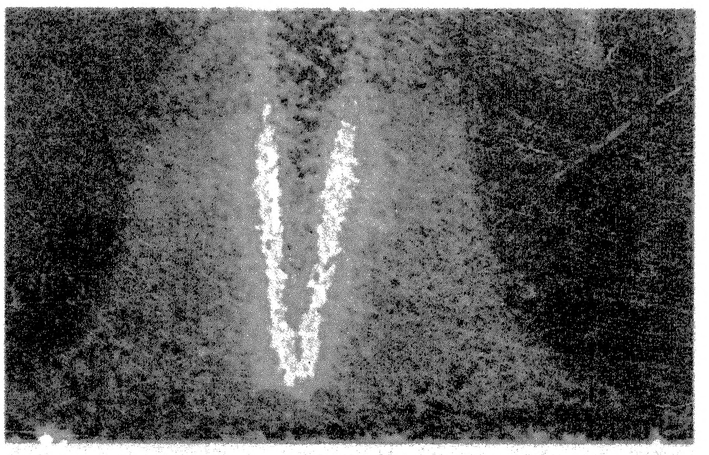

FIG. 10. CH LIF distribution during diamond deposition (T_s=1000 °C, d=0.67 mm, and S_{ac}=5%). Reflections of the laser beam off the diamond facets are not completely blocked. The substrate is indicated in yellow; the image is 8 mm wide.

looks similar to the C_2 LIF distribution, but certain differences can be observed.

In the same way as for C_2, the thickness δ_{BL} of the boundary layer is determined and horizontal intensity profiles are taken at a distance δ_{BL} above the substrate surface, see Figs. 11 and 12, respectively. From Fig. 11 it can be seen that δ_{BL} does not change significantly with T_s, as for C_2, and that δ_{BL} clearly increases with increasing d. Due to the noise, the trend in the horizontal profiles, given in Fig. 12, is less clear than for C_2, but evidently no maximum is observed at the symmetry axis of the flame for d > 1.5 mm.

The spatial distribution of natural CH emission shows the same features as the CH LIF spatial distribution. Similarly to C_2, it is confined to a smaller area than the LIF distribution. This also follows from Fig. 11, which shows that δ_{BL} is smaller for the CH LIF signal than it is for the CH natural flame emission.

3. Non-resonant fluorescence

Although the non-resonant background, excited around 393 nm, is undesirable in spectroscopic measurements, it can be of use in determining and controlling the supersaturation of acetylene in the flame. Figure 13 shows the non-resonant fluorescence intensity recorded in a square area of 1.0 mm^2, 1.5 mm off the symmetry axis of the flame, well outside the conical flame front. This area is inside the acetylene feather if the flame is fuel-rich. The oxygen flow is fixed at 2.84 SLM and the acetylene flow is varied slightly to change

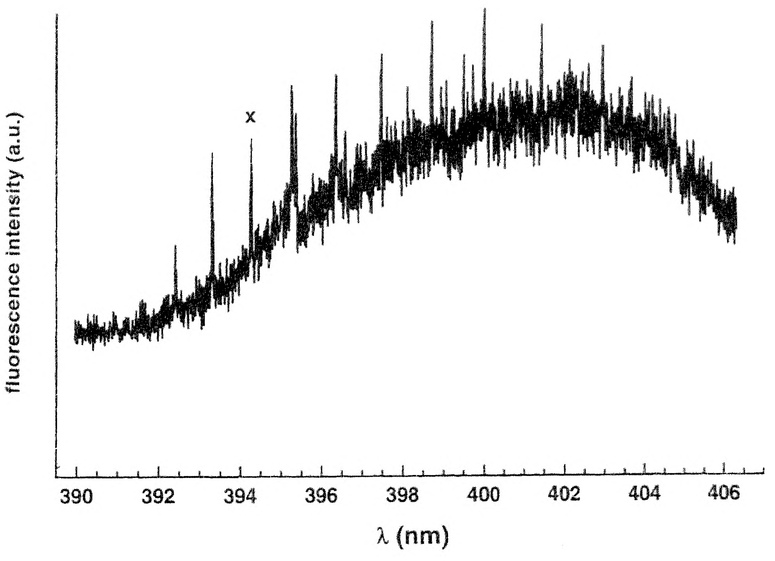

FIG. 9. CH excitation spectrum recorded at the tip of the flame front during diamond deposition. The transition marked with 'x' is used for imaging. The large background is due to non-resonant fluorescence and is proportional to the laser power.

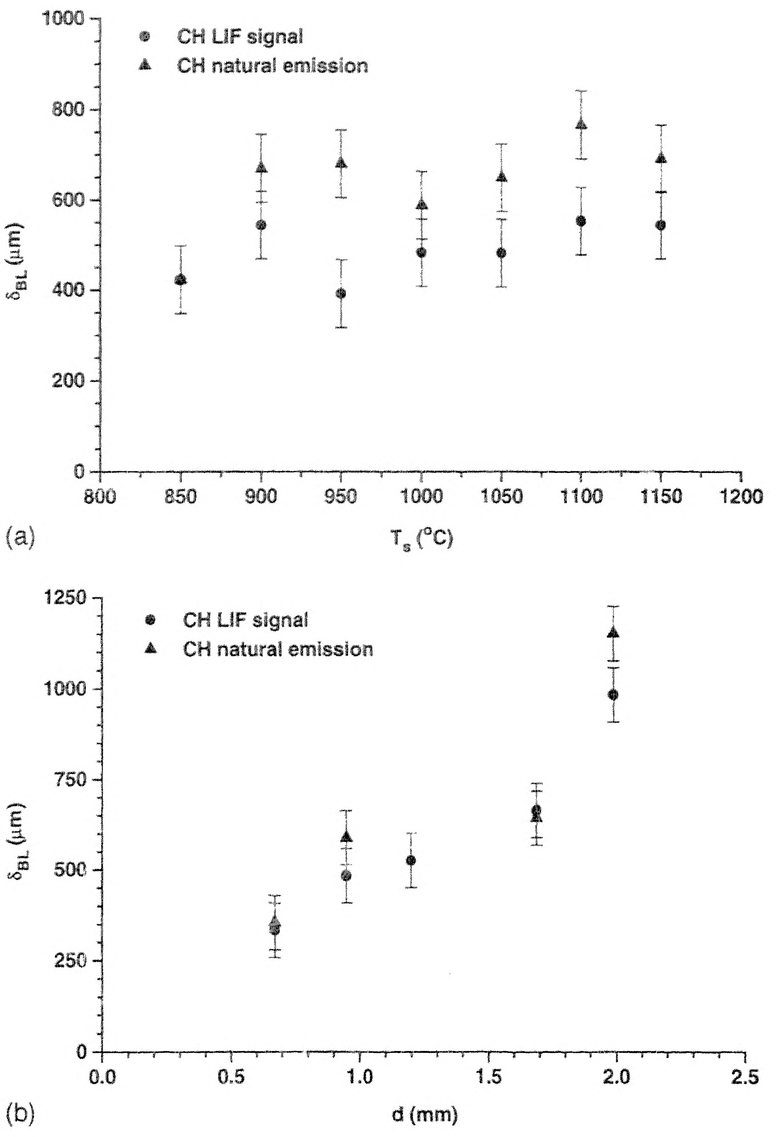

FIG. 11. Dependence of the thickness of the boundary layer δ_{BL} on (a) the temperature T_s and (b) the distance d for CH LIF and natural CH emission of the flame.

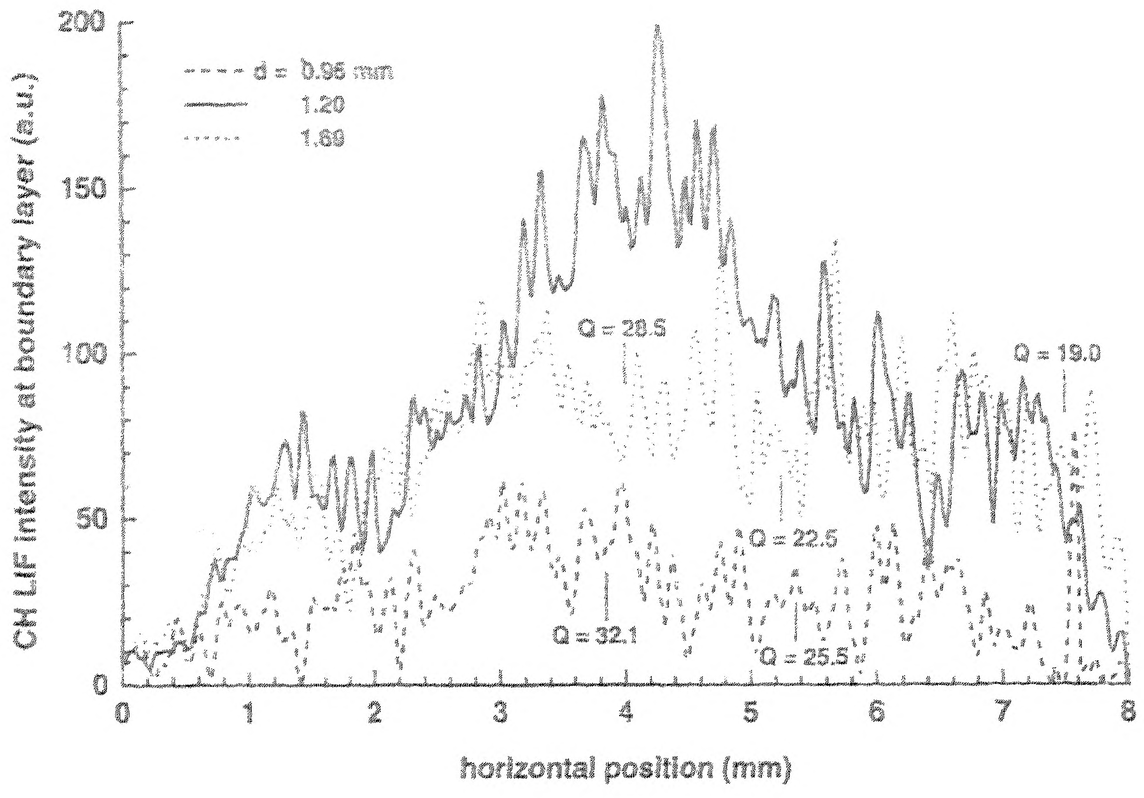

FIG. 12. Horizontal CH LIF intensity profiles at a distance δ_{BL} above the substrate, for different deposition distances; $T_s = 1000$ °C. Q is the quality factor of the diamond deposit at the corresponding position at the substrate.

the flame from fuel-rich to oxygen-rich conditions. The neutral flame is observed by sight to occur at an acetylene flow of 2.58 SLM. Under oxygen-rich combustion conditions there is no acetylene feather and no non-resonant fluorescence is recorded in the selected area. Under fuel-rich conditions the signal appears to increase linearly with the acetylene flow, starting only to saturate at very high acetylene flow rates, where the flame changes to a long, yellow, sooting flame. In order to determine the transition from oxygen-rich to fuel-rich conditions, i.e., the occurrence of the neutral flame, two separate linear fits are made: one for the data in the oxygen-rich and one for the data in the fuel-rich regime. The intersection of the two linear fits turns out to correspond to an acetylene flow of 2.58±0.01 SLM, which is the flow for the neutral flame. In this way the somewhat inaccurate determination by sight of the neutral flame can be replaced by the accurate determination by non-resonant fluorescence detection in the acetylene feather. Once the desired value of

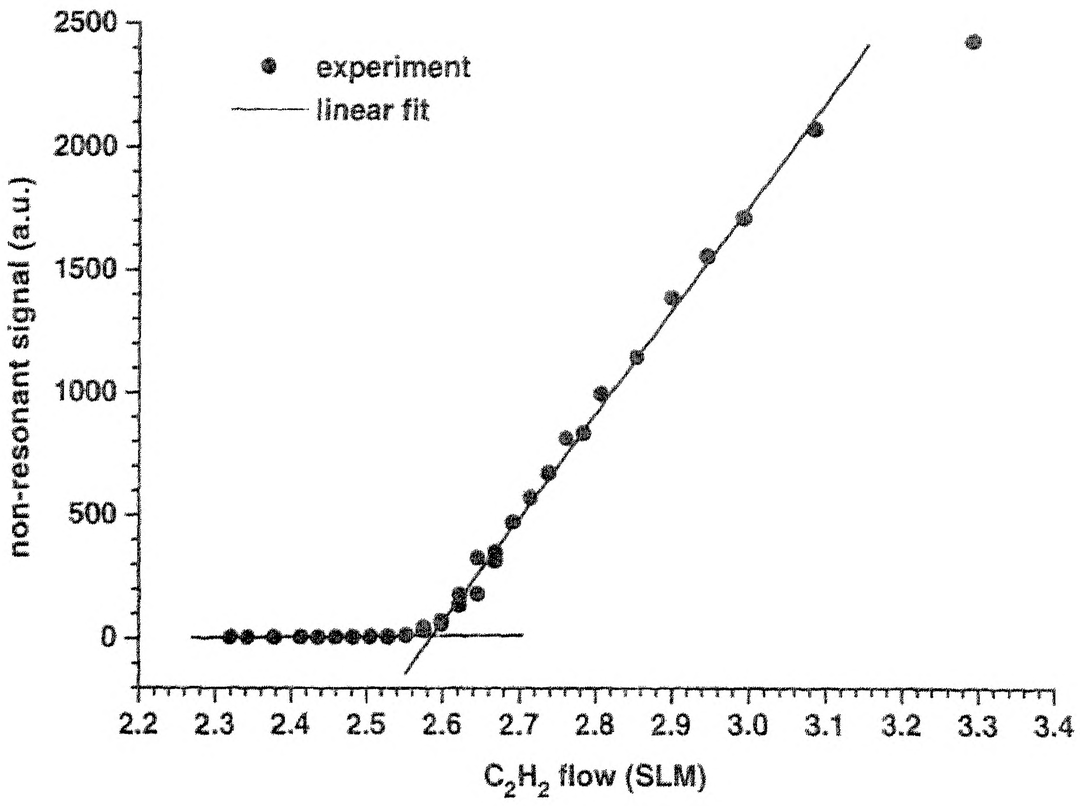

FIG. 13. Non-resonant fluorescence signal detected in the flame, 1.5 mm off the symmetry axis. The oxygen flow is constant at 2.84 SLM. The intersection of the two linear fits corresponds to the neutral flame as determined by sight.

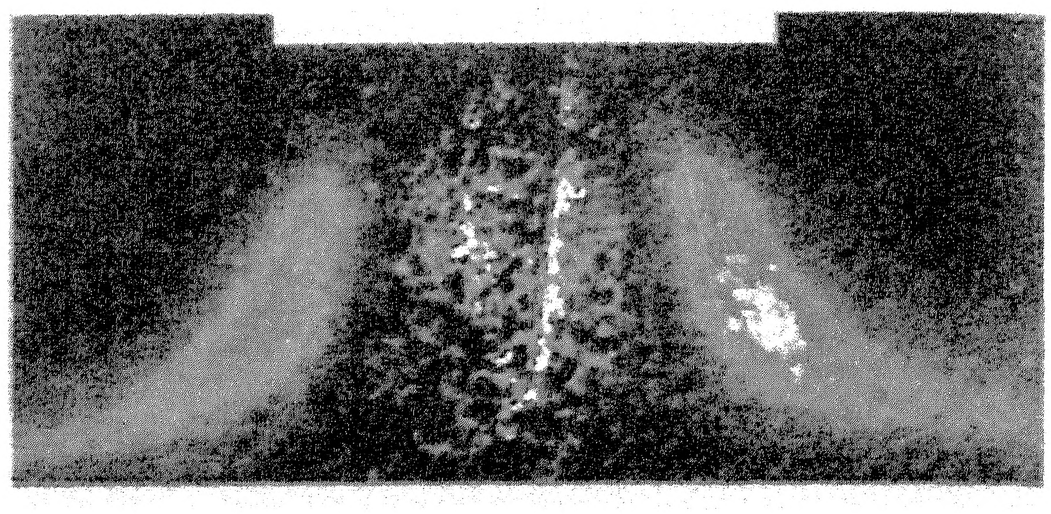

FIG. 14. OH LIF distribution during diamond deposition ($T_s = 1000$ °C, d=0.9 mm, and $S_{ac}=6\%$). The signal at the flame front is non-resonant fluorescence, OH LIF signal is only visible in the two lobes. The tip of the burner and the substrate are indicated in yellow; the image is 14 mm wide.

S_{ac} is adjusted when starting a deposition experiment, the absolute non-resonant fluorescence intensity can be used as a feedback signal to keep S_{ac} constant during diamond growth, with a far better accuracy than is possible by observation by sight.

4. OH

The two-dimensional distribution of OH during diamond deposition is shown in Fig. 14. Deposition conditions are $T_s = 1000$ °C, d=0.9 mm, and $S_{ac}=6\%$. OH is excited at 308 nm and detected at 343 nm. A very large LIF signal is obtained from the outer lobes, located outside the visible flame. As expected, the signal intensity in the lobes hardly changes as the flame is varied from oxygen-rich to fuel-rich, because OH in this region is created by reactions of combustion products with ambient air. The OH LIF signal is observed in the region between the lobes and the flame front only if the flame is oxygen-rich. In a fuel-rich flame, already at supersaturations of a few percent, the OH LIF signal is very difficult to observe. In Fig. 15 the signal intensity just above the substrate is compared to the intensity in the lobes. In this case OH is excited at 282 nm and fluorescence is detected with the camera system at 312 nm, in order to make use of a

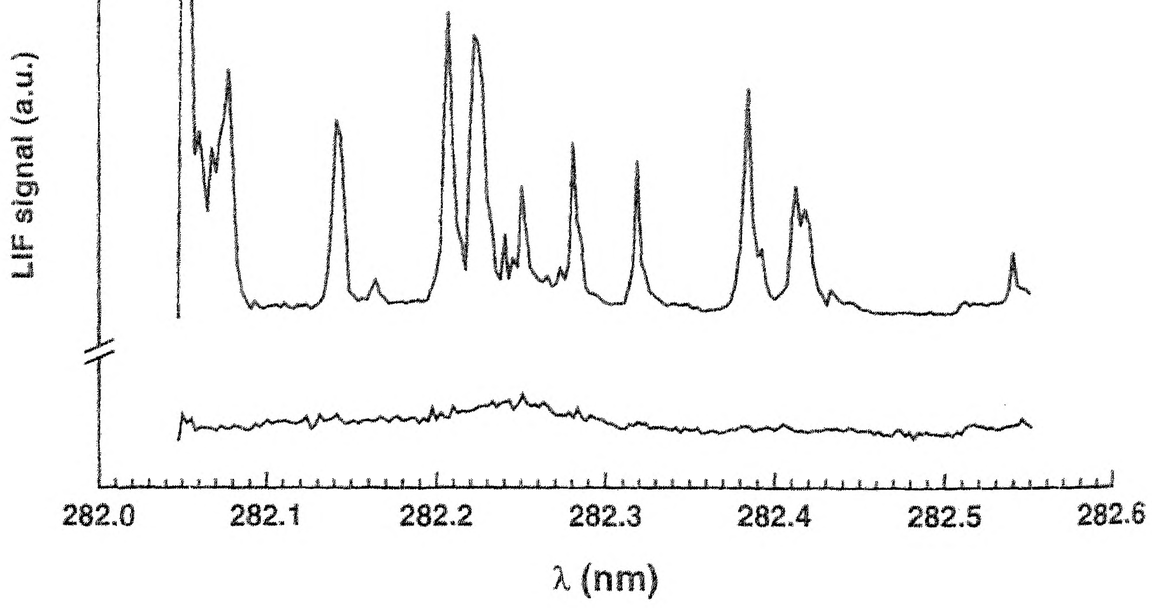

FIG. 15. Part of the OH excitation spectrum around 282 nm (with detection at 312 nm). Simultaneous recordings in the outer lobes (upper trace) and just above the substrate at the symmetry axis (lower trace) in a diamond depositing flame ($S_{ac}=6\%$).

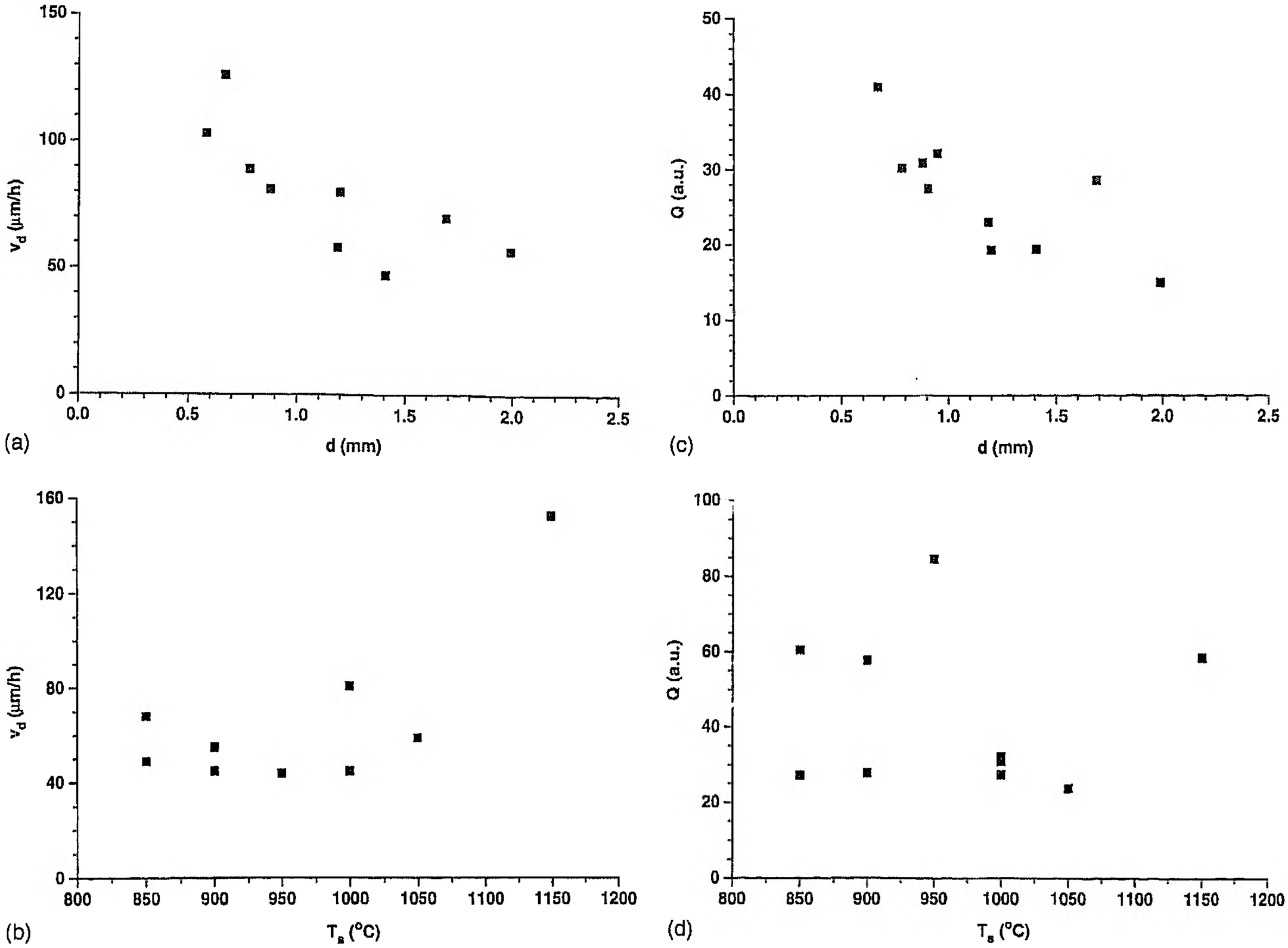

FIG. 16. Growth rate (a,b) and quality factor (c,d) as a function of distance and temperature for all deposited diamond layers.

stronger fluorescence transition. But even then hardly any OH LIF signal can be detected just above the substrate, while the signal in the lobes is again very strong. Only at 282.25 nm weak OH fluorescence is observed. Measurements of OH with excitation at 248 nm give the same results, indicating that it will be very difficult to perform OH rotational temperature measurements by the laser induced predissociative fluorescence (LIPF) technique in the flame and the boundary layer under diamond deposition conditions.

The very low OH LIF intensity inside the acetylene feather seems to contradict other experiments, in which readily detectable amounts of OH natural emission are measured at positions in the flame where good quality diamond is deposited onto the substrate.[6,7] This contradiction may arise from the fact that optical emission spectroscopy (OES) is a line of sight integrating technique, whereas the two-dimensional LIF detection gives a real cross section of the area of interest.

Temperature calculations from excitation spectra of C_2 or CH are not carried out, because collisional quenching of fluorescence, which plays a dominant role in this atmospheric pressure flame, is not quantitatively known. For CH also the energy transfer rate between the $B^2\Sigma^-$ and the $A^2\Delta$ states is not sufficiently well known.

B. Relation to diamond growth

The growth rate v_d, Raman spectra, and the quality factor Q are determined for all samples after growth. The behavior of v_d and Q as a function of T_s and d is shown in Fig. 16, where v_d and Q are the maximum values measured for each deposited diamond layer. The results are similar to those obtained with the same setup in a previous study,[20] although absolute values are not completely comparable due to slightly different deposition conditions and differences in the Raman equipment. Figures 16(a) and 16(b) show that v_d decreases with increasing d and increases with increasing T_s. Although Q shows a radial variation within a single diamond layer, as will be discussed below, Fig. 16(c) shows Q decreasing with increasing d. The dependence of Q on T_s, presented in Fig. 16(d), is less clear.

In Fig. 17 a photograph of one deposited diamond layer is presented. All deposits show a rather uniformly covered central area of about 7 mm ϕ, consisting of crystallites which mainly reveal {111} facets. For d<1 mm, the area right beneath the tip of the flame front, about 1.8 mm in diameter, exhibits higher v_d than the rest of the central area and sometimes breaks up into separate crystallites. In moving outwards from the center of the deposit, the central region changes into an annular region showing mainly {100} facets.

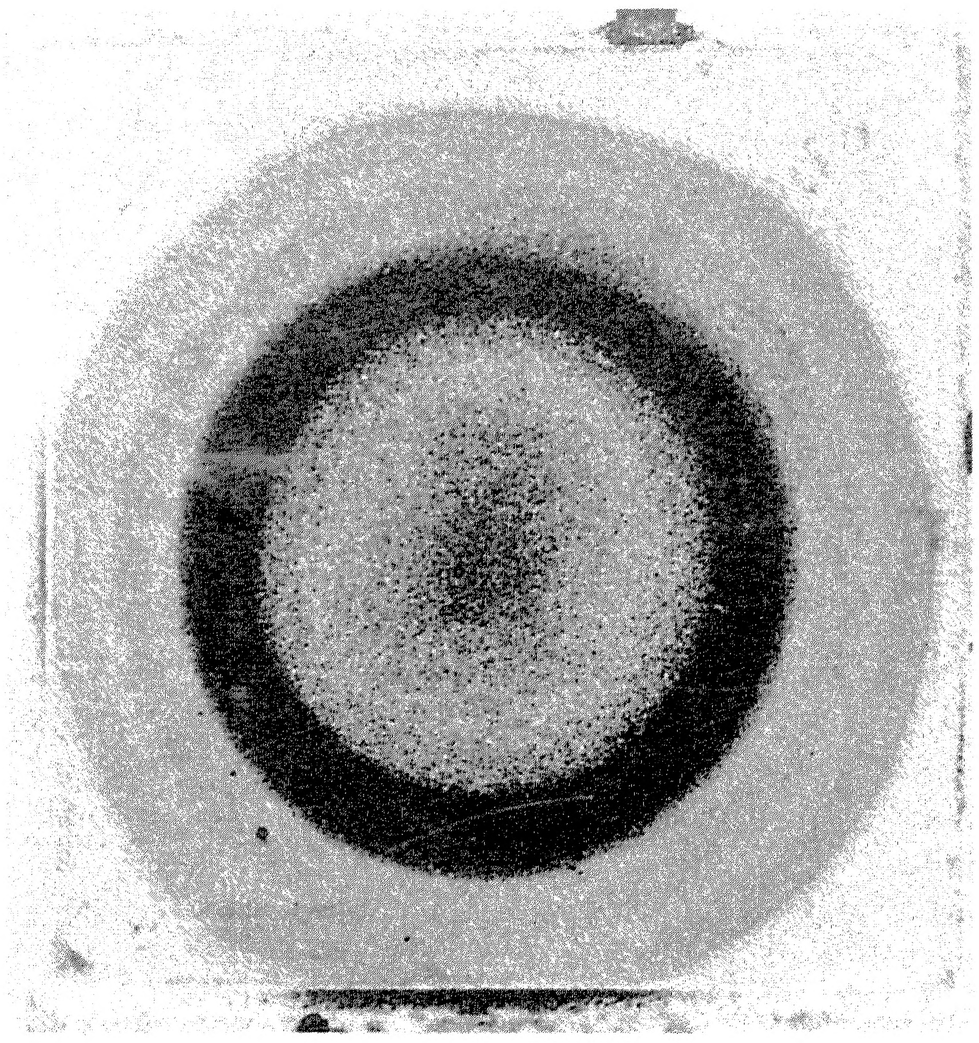

FIG. 17. Photograph of a typical diamond layer. Deposition conditions are: $T_s = 1000$ °C, d=0.78 mm, and $S_{ac} = 5\%$. The molybdenum square is 13 mm ×13 mm.

Further outside this annulus a non-diamond carbon deposit is found and sometimes even further outwards a very narrow ring (varying from 8.5 to 10 mm in diameter and less than 0.1 mm wide) of crystallites with {100} facets can be seen.

For two specific diamond layers, v_d is determined at equidistant points along two lines passing through the center of the deposit. One line is parallel to the direction of the laser beam during the LIF measurements, the other perpendicular to the laser beam. The results are given in Fig. 18, with $T_s = 1000$ °C and d=0.88 mm and 1.41 mm, respectively, the deposition conditions. The corresponding horizontal C_2 intensity profiles are the top and bottom ones in Fig. 7. Upon comparison of the C_2 intensity profile to the v_d profile for d=1.41 mm, it is clear that both are nearly flat across the diamond layer. The v_d profile measured in the direction of the laser beam even shows a shallow minimum around the center of the deposit, similar to the C_2 intensity profile. The C_2 intensity profile and the v_d profile for d=0.88 mm, however, both show a clear maximum with about the same gradient at the center of the diamond layer. The small increase of v_d further outwards is also observed for other diamond layers deposited at d<1 mm and corresponds to the transition of the uniformly covered area to the annular region with mainly {100} facets. In the C_2 intensity profile, however, no increase is observed outside the center.

Figure 19 shows the Raman spectra and Q values of one specific diamond deposit for three points on a radial line starting at the center. In this way Q values are obtained for all samples. In Figs. 7 and 12 Q values are presented for radially different positions of those samples for which horizontal profiles are obtained during deposition. In Fig. 7 a relation is observed between the Q value at a certain position at the diamond surface and the C_2 density in the boundary layer immediately above it. For d < 1 mm both Q and the C_2 density show a maximum at the center of the deposited layer and both decrease in moving radially away from the

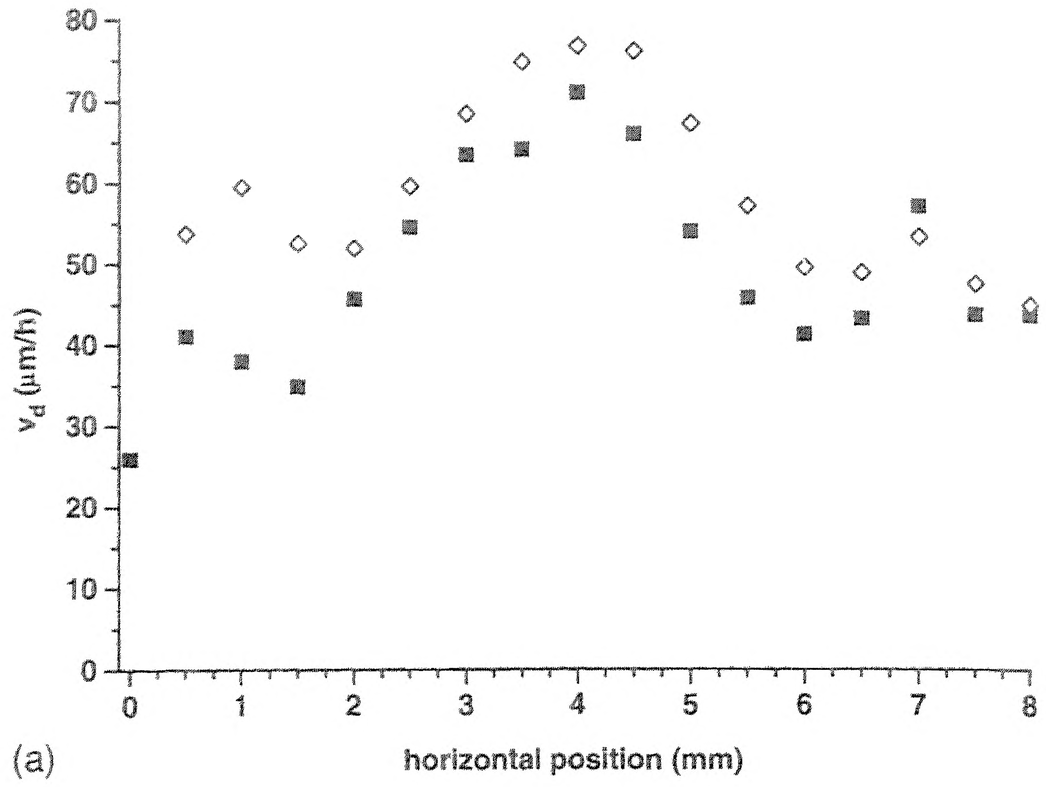

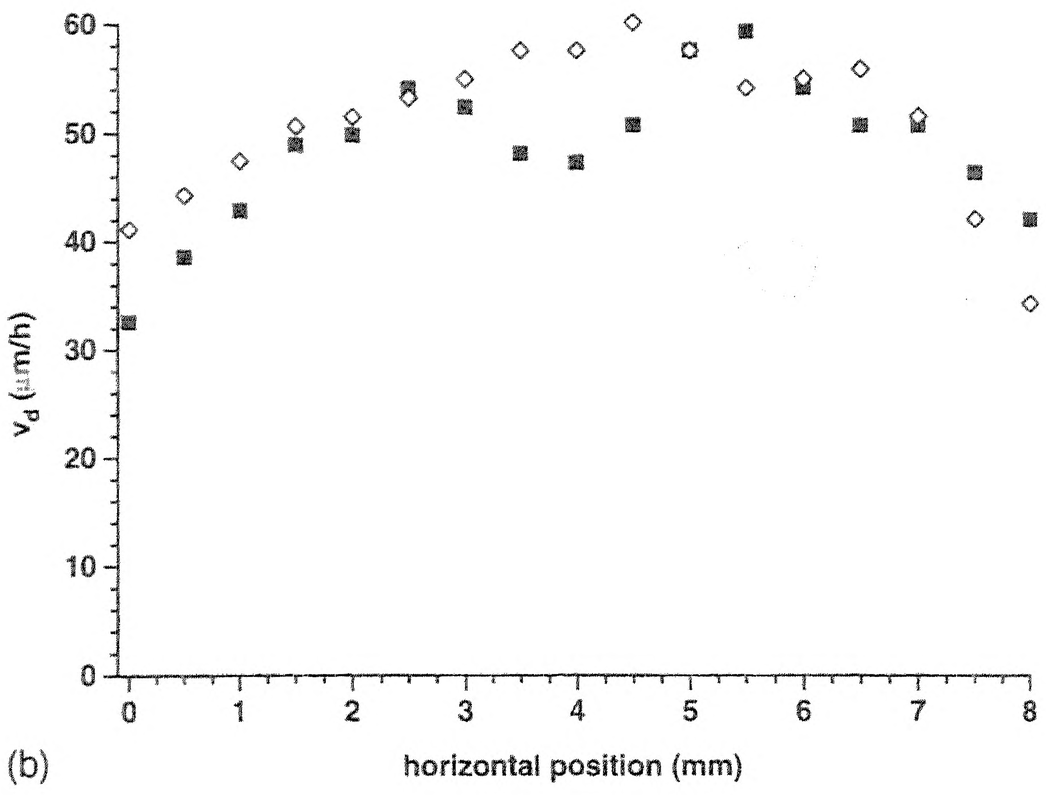

FIG. 18. Local growth rate variation within a single diamond layer, along a line passing through the center. Filled symbols: parallel to the laser sheet; open symbols: perpendicular to the laser sheet. Deposition conditions are those of Fig. 7, with d=0.88 mm (a) and d=1.41 mm (b).

center. For d > 1 mm, however, Q shows a local minimum at the center of the deposited layer, similar to the C_2 density distribution. For the horizontal profiles of the CH LIF boundary layer, presented in Fig. 12, the relation with Q is less clear due to the noise.

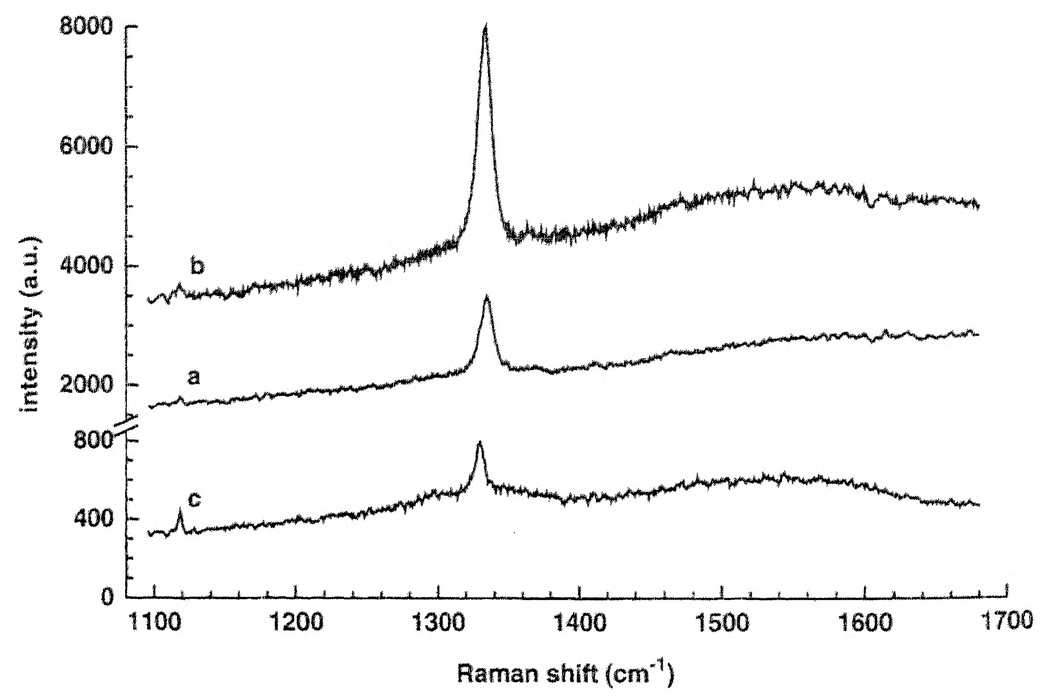

FIG. 19. Raman spectra obtained for three different positions on a single deposited layer: (a) at the center: r=0.0 mm, Q=11.9; (b) outside the center: r=1.5 mm, Q=19.3; (c) at the edge of the annular region: r=3.5 mm, Q=8.6. Deposition conditions are those of Fig. 7, bottom trace.

When the dimensions of the regions with different morphology in the diamond layer, as described above, are compared to the lateral dimensions of the C_2, CH, and OH LIF distributions, shown in Figs. 5, 10, and 14, respectively, it becomes clear that the size of the uniformly covered central area corresponds to the width of the acetylene feather, which is about 7 mm at the substrate. The surrounding annular region with {100} facets is formed at the edge of the acetylene feather, which is also the border of the ground state C_2 and CH distributions. Outside this region OH is strongly present and Q decreases further or becomes impossible to determine. The very narrow ring of crystallites with {100} facets sometimes occurring is located just outside the acetylene feather.

IV. CONCLUSIONS

The two-dimensional LIF detection technique has been applied to a diamond depositing oxyacetylene flame to measure the distributions of C_2, CH, and OH. Two-dimensional density distributions have been measured with high spatial resolution and during diamond deposition onto the substrate, thus allowing *in situ* diagnostics of the gas phase above the substrate.

Special attention has been given to the dark boundary layer, typically a few hundreds of microns thick, which is observed just above the substrate for both C_2 and CH, in natural emission of the flame as well as in laser induced fluorescence. The thickness of the boundary layer does not appear to depend very strongly on the substrate temperature and the distance between the flame front and the substrate, except for CH, where the boundary layer thickness increases if the distance is increased. From the definition of the boundary layer thickness in this work, it is clear that it is a relative measure of the rate of decrease in density of the investigated species: a thin boundary layer corresponds to a large density gradient and a thick boundary layer indicates a small density gradient. So if the substrate temperature is increased, corresponding to a slight increase in the diamond deposition rate, the CH-to-C_2 density ratio remains constant. But if the distance of the flame front to the substrate is increased, resulting in a lower deposition rate and a lower quality of the diamond, the CH-to-C_2 density ratio decreases.

A relation is observed between the C_2 density distribution in the boundary layer and the local variation of the growth rate across a single diamond layer. The growth rate is nearly constant over the central area if the C_2 density distribution is nearly flat, and exhibits a central maximum if the C_2 distribution peaks at the center. The local increase of the growth rate near the annular region with {100} facets cannot be explained by this relation, but might be due to the interaction between the acetylene feather and the ambient air.

Another relation is observed between the quality of the deposited diamond and the C_2 density distribution in the boundary layer, in which a higher C_2 density corresponds to a higher quality at the corresponding position at the diamond surface. For CH no such relations with the diamond growth rate and quality are found. This, however, might also be due to the low signal to noise ratio obtained for CH.

Flame deposition experiments carried out by Schermer and co-workers[29] under similar conditions, but with a larger distance (up to ≈ 10 mm) between substrate and flame front, show a high non-diamond carbon content and therefore a smaller Q value in the central region of the diamond layer. The diameter of this region is comparable to the width of the central minimum in the horizontal C_2 LIF profiles measured in this work. Cappelli and Paul[9] performed flame deposition experiments of diamond onto a silicon substrate, with comparable distances between burner and substrate. They found diamond deposition to occur only in an annular region, whereas the center of their deposits showed a high non-diamond carbon content.

Combined with the behavior of the boundary layer, this suggests that C_2 is an important precursor for diamond growth. The importance of C_2 for diamond growth is also described by Gruen and co-workers,[30,31] who deposited diamond films in a hydrogen free environment, using fullerene precursors in an argon microwave plasma. They found C_2 in their system to originate from the dissociation of C_{60} and explain their obtained relatively high deposition rate with direct C_2 adsorption to the diamond surface and conclude it is the main growth species in their system. In the work presented here indications have also been obtained that CH seems to be important for diamond growth.

In general it has been found that the deposition of a closed polycrystalline diamond layer is restricted to the area covered by the acetylene feather. Ground state and excited state C_2 and CH are found to be present in the feather in readily detectable quantities, but OH is barely detectable inside the feather. Okada *et al.*[7] conclude from their OES measurements that OH radicals "exist adequately in the acetylene feather" and suggest, like Cappelli and Paul,[9] that OH is important for diamond growth. In contrast to this, the OH LIF measurements presented in this work suggest that the role of OH, in hydrogen abstraction at the diamond surface and graphite etching during deposition, is of minor importance. OH has been detected, however, outside the acetylene feather, where the fluorescence signal is found to be nearly independent of combustion conditions over a range which is much wider than that for which diamond deposition is possible. This contradicts the OES measurements of Hirose *et al.*,[6] who found a rather strong dependence of the diamond quality on the OES signal of OH. Most probably the OES signal of OH originates from the area outside the acetylene feather.

The observed non-resonant fluorescence signal, excited around 393 nm, turns out to be directly proportional to the acetylene supersaturation. This allows a more accurate adjustment of the supersaturation, a critical parameter in the deposition process, than is possible by sight.

Finally, it is clear that an elaborate, two-dimensional model of the flame deposition process of diamond is needed in order to calculate the behavior of the boundary layer and the density distributions of various species found therein.

ACKNOWLEDGMENTS

The authors wish to thank Ir. J.J. Schermer for useful discussions and his help with the Raman equipment, and also Professor L.J. Giling, Dr. W.J.P. van Enckevort, Dr. G. Janssen and W.A.L.M. Elst for many useful discussions. This

work has been made possible by financial support of the Stichting voor Technische Wetenschappen (Technology Foundation) and partial financial support by the European Community Brite Euram project BE 5099-92 under contract BRE-2-0147.

[1] Y. Hirose and N. Kondo, Extended Abstracts, 35th Jpn. Appl. Phys. Spring Meeting, March 1988, p. 434.
[2] K.A. Snail and L.M. Hanssen, J. Cryst. Growth **112**, 651 (1991).
[3] J.J. Schermer, W.J.P. van Enckevort, and L.J. Giling, Diamond Rel. Mater. **3**, 408 (1994).
[4] K.A. Snail, R.G. Vardiman, J.P. Estrera, J.W. Glesener, C. Merzbacher, C.J. Craigie, C.M. Marks, R. Glosser, and J.A. Freitas, J. Appl. Phys. **74**, 7561 (1993).
[5] Y. Matsui, H. Yabe, T. Sugimoto, and Y. Hirose, Diamond Rel. Mater. **1**, 19 (1991).
[6] Y. Hirose, S. Amanuma, and K. Komaki, J. Appl. Phys. **68**, 6401 (1990).
[7] K. Okada, S. Komatsu, T. Ishigaki, S. Matsumoto, and Y. Moriyoshi, J. Appl. Phys. **71**, 4920 (1992).
[8] Y. Matsui, A. Yuuki, M. Sahara, and Y. Hirose, Jpn. J. Appl. Phys. **28**, 1718 (1989).
[9] M.A. Cappelli and P.H. Paul, J. Appl. Phys. **67**, 2596 (1990).
[10] Y. Liou and Y.-R. Ma, Diamond Rel. Mater. **3**, 573 (1994).
[11] D.S. Green, T.G. Owano, S. Williams, D.G. Goodwin, R.N. Zare, and C.H. Kruger, Science **259**, 1726 (1993).
[12] G.A. Raiche and J.B. Jeffries, Appl. Opt. **32**, 4629 (1993).
[13] M. Chenevier, J.C. Cubertafon, A. Campargue, and J.P. Booth, Diamond Rel. Mater. **3**, 587 (1994).
[14] D.P. Dowling, T.P. O'Brien, E.M. Davitt, K. Donelly, T.C. Kelly, H.F. Doebele, V. Kornas, W.G. Graham, R. Cheshire, M. Higgins, and T. Morrow, Diamond Rel. Mater. **3**, 702 (1994).
[15] Y. Matsui, H. Yabe, and Y. Hirose, Jpn. J. Appl. Phys. **29**, 1552 (1990).
[16] D.G. Goodwin, Appl. Phys. Lett. **59**, 277 (1991).
[17] M. Versluis, M. Boogaarts, R. Klein-Douwel, B. Thus, W. de Jongh, A. Braam, J.J. ter Meulen, W.L. Meerts, and G. Meier, Appl. Phys. B **55**, 164 (1992).
[18] A.D. Sappey, D.R. Crosley, and R.A. Copeland, Appl. Phys. B **50**, 463 (1990).
[19] Th.M. Brugman, R. Klein-Douwel, G. Huigen, E. van Walwijk, and J.J. ter Meulen, Appl. Phys. B **57**, 405 (1993).
[20] J.J. Schermer, J.E.M. Hogenkamp, G.C.J. Otter, G. Janssen, W.J.P. van Enckevort, and L.J. Giling, Diamond Rel. Mater. **2**, 1149 (1993).
[21] J.J. Schermer (private communication).
[22] R.W.B. Pearse and A.G. Gaydon, *The Identification of Molecular Spectra* (Chapman & Hall, London, 1976).
[23] N.L. Garland, and D.R. Crosley, Appl. Opt. **24**, 4229 (1985).
[24] J. Hinze, G.C. Lie, and B. Liu, Ap. J. **196**, 621 (1975).
[25] J. Brzozowski, P. Bunker, N. Elander, and P. Erman, Ap. J. **207**, 414 (1976).
[26] P. Andresen, A. Bath, W. Gröger, H. Lülf, G. Meijer, and J.J. ter Meulen, Appl. Opt. **27**, 365 (1988).
[27] A.G. Gaydon and H.G. Wolfhard, *Flames, Their Structure, Radiation and Temperature* (Chapman & Hall, London, 1979), pp. 220 and 231.
[28] In Ref. 27, p. 221.
[29] J.J. Schermer, W.A.L.M. Elst, and L.J. Giling, Diamond Rel. Mater. (in press, 1995).
[30] D.M. Gruen, S. Liu, A.R. Krauss, and X. Pan, J. Appl. Phys. **75**, 1758 (1994).
[31] D.M. Gruen, S. Liu, A.R. Krauss, J. Luo, and X. Pan, Appl. Phys. Lett. **64**, 1502 (1994).